Cell Death and Differentiation (2014) 21, 258–269

www.nature.com/cdd

Therapeutic targeting of constitutive PARP activation compromises stem cell phenotype and survival of glioblastoma-initiating cells

M Venere[1,6], P Hamerlik[2,3,6], Q Wu[1], RD Rasmussen[2], LA Song[1], A Vasanji[4], N Tenley[4], WA Flavahan[1], AB Hjelmeland[1,5], J Bartek*[,2,3] and JN Rich*[,1,5]

Glioblastoma-initiating cells (GICs) are self-renewing tumorigenic sub-populations, contributing to therapeutic resistance via decreased sensitivity to ionizing radiation (IR). GIC survival following IR is attributed to an augmented response to genotoxic stress. We now report that GICs are primed to handle additional stress due to basal activation of single-strand break repair (SSBR), the main DNA damage response pathway activated by reactive oxygen species (ROS), compared with non-GICs. ROS levels were higher in GICs and likely contributed to the oxidative base damage and single-strand DNA breaks found elevated in GICs. To tolerate constitutive DNA damage, GICs exhibited a reliance on the key SSBR mediator, poly-ADP-ribose polymerase (PARP), with decreased viability seen upon small molecule inhibition to PARP. PARP inhibition (PARPi) sensitized GICs to radiation and inhibited growth, self-renewal, and DNA damage repair. *In vivo* treatment with PARPi and radiotherapy attenuated radiation-induced enrichment of GICs and inhibited the central cancer stem cell phenotype of tumor initiation. These results indicate that elevated PARP activation within GICs permits exploitation of this dependence, potently augmenting therapeutic efficacy of IR against GICs. In addition, our results support further development of clinical trials with PARPi and radiation in glioblastoma.
Cell Death and Differentiation (2014) **21,** 258–269; doi:10.1038/cdd.2013.136; published online 11 October 2013

Glioblastomas (World Health Organization grade IV gliomas) rank among the most lethal of human cancers. Median survival remains 12–15 months despite recent advances in the standard-of-care, which includes maximal surgical resection followed by concurrent radiotherapy and chemotherapy with the DNA-alkylating agent temozolomide.[1] Radiation is the most effective non-surgical therapy for glioblastoma but recurrence is essentially universal. Failure of sustained tumor control by radiation reflects numerous causes, including the recent implication of intratumoral heterogeneity. In parallel to other cancers, we and others have identified highly tumorigenic sub-populations within gliomas, designated as tumor-initiating cells (TICs) based on the preferential ability of these cells to propagate secondary tumors that phenocopy the original tumor.[2] Although the cancer stem cell hypothesis remains controversial because of the evolving understanding of cellular plasticity and use of markers, many studies have demonstrated that glioblastomas contain cellular hierarchies with the self-renewing glioblastoma-initiating cells (GICs) at the apex.[2–7] GICs are therapeutically important because they are relatively resistant to radiation and conventional chemotherapy,[2,8] promote tumor angiogenesis,[9] and invade into normal tissues.[10] Direct evidence of GIC resistance in human patients was demonstrated by expansion of GICs following external-beam radiation therapy and Gamma Knife treatment.[11] Thus, effective killing of GICs may improve tumor progression/growth control through multiple mechanisms.[12]

Effective targeting of GIC resistance requires elucidation of the molecular mechanisms underlying the ability of these cells to survive and repopulate tumors after radiation.[13] In our early studies, we found that GICs have higher basal activation of components of the DNA damage response (DDR) as well as more pronounced DDR activation following irradiation that contribute to greater survival over non-GICs.[2] Targeting key kinases activated by DNA damage and involved in checkpoint activation, Chk1 and Chk2, with a small molecule inhibitor radiosensitizes GICs.[2] Further studies have provided additional molecular mechanisms of GIC radioresistance,

[1]Department of Stem Cell Biology and Regenerative Medicine, Lerner Research Institute, Cleveland Clinic Foundation, 9500 Euclid Ave NE30 9500 Euclid Ave, Cleveland, OH 44195, USA; [2]Genome Integrity Unit, Danish Cancer Society Research Center, Strandboulevarden 49, Copenhagen DK-2100, Denmark; [3]Laboratory of Genome Integrity, Institute of Molecular and Translational Medicine, Faculty of Medicine and Dentistry, Palacky University, Hnevotinska 5, Olomouc CZ-775 15, Czech Republic; [4]ImageIQ Inc., Cleveland, OH 44106, USA and [5]Department of Molecular Medicine, Cleveland Clinic Lerner College of Medicine at Case Western Reserve University, Cleveland, OH 44106, USA

*Corresponding authors: J Bartek, Genome Integrity Unit, Danish Cancer Society Research Center, Strandboulevarden 49, Copenhagen DK-2100, Denmark. Tel: +45 35 25 73 57; Fax: +45 35 25 7721; E-mail: jb@cancer.dk

or JN Rich, Department of Stem Cell Biology and Regenerative Medicine, Lerner Research Institute, Cleveland Clinic, 9500 Euclid Ave NE30 9500 Euclid Ave, Cleveland, OH 44118, USA. Tel: +1 216 636 0790; Fax: +1 216 636 5454; E-mail: richj@ccf.org

[6]These authors contributed equally to this work.

Keywords: cancer stem cell; DNA repair; glioma; radioresistance; PARP

Abbreviations: PARP, poly-ADP-ribose polymerase; GIC, glioblastoma-initiating cell; IR, ionizing radiation; SSBR, single-strand break repair; TIC, tumor-initiating cell; DDR, DNA damage response; ROS, reactive oxygen species; GFAP, glial fibrillary acidic protein; Gy, Gray; ATP, adenosine triphosphate; PARPi, PARP inhibition

Received 04.4.13; revised 08.8.13; accepted 14.8.13; Edited by P Salomoni ; published online 11.10.2013

including SirT1,[14] Notch,[15] STAT3,[16] VEGF/VEGFR2,[17] BMI1,[18] L1CAM,[19] and peroxiredoxin-1.[20] Altogether, these studies highlight a radioresistance phenotype for GICs, a potential direct contribution to tumor recurrence, and the prospect of targeting these cells through inhibition of molecular targets including the DDR.

One of the crucial determinants of genome integrity and cellular response to DNA damage is the level of intracellular reactive oxygen species (ROS), which is tightly regulated through the coordinated activities of cellular pro-oxidants/antioxidants and results in the induction of DNA single-strand breaks (SSBs). The role of single-strand break repair (SSBR) in GICs remains unexplored. This mode of DNA repair is utilized by cells in response to ROS generated by cellular metabolism or exogenous sources such as ionizing radiation (IR). Central to the detection and resolution of these lesions is poly-ADP-ribose polymerase 1 (PARP1). PARP1 catalyzes the transfer of ADP-ribose polymers to downstream substrates including numerous DNA repair enzymes, facilitating DNA repair. *In vitro*, inhibitors to PARP1 (often targeting both PARP1 and PARP2, and herein termed PARP inhibitors) radiosensitize cancer cells, including glioma cell lines, to drug and radiation treatment.[21–27] *In vivo*, PARP inhibitors enhance radiation therapy in syngeneic and xenograft models for colon, lung, head and neck, and cervical cancers.[21,28–32] Olaparib (AZD2281), which targets PARP1 and PARP2, is currently in several phase I and phase II trials for solid tumors as a single agent or in combination with chemotherapy and/or radiotherapy.[33] A phase I study is ongoing for olaparib plus temozolomide in patients with relapsed GBM (http://www.clinicaltrials.gov). Here, we sought to further our understanding of SSBR within GICs and evaluate the therapeutic potential of targeting SSBR through PARP inhibition (PARPi).

Results

Increased ROS and base damage in GICs correlates with increased activity of the SSBR mediator, PARP1. Although we have previously shown high and variable levels of oxidative DNA lesions in biopsies of human glioblastomas,[34] there have been no such studies in GICs *versus* non-GIC. We first evaluated the baseline ROS levels in low-passage GICs derived from human glioblastoma specimens previously validated to fulfill functional criteria of GICs: self-renewal, sustained proliferation, stem cell marker expression, capacity for lineage commitment, and tumor propagation.[2,35–37] Using flow cytometry on acutely dissociated xenografts, GICs demonstrated higher ROS levels when compared with matched non-GICs (Figure 1a, Supplementary Figure 1a). Evaluation of ROS immediately following tumor dissociation was essential as query of publically available array data from increasingly passaged xenograft specimens[38] found genes previously reported to be differentially expressed in breast cancer TICs[39] to have altered expression upon continual passage (Supplementary Figure 2). Total adenosine triphosphate (ATP) levels, a representation of metabolic activity, were significantly higher in GICs than that in non-GICs, supporting differential metabolic states as a contributing factor to the increased ROS levels in GICs (Supplementary Figure 3a). The main impact of ROS production is the generation of base lesions and DNA SSBs. The GIC population had higher oxidative base damage, as measured by levels of 8-oxo-2′-deoxyguanosine base modifications, in all tumor models evaluated (Figure 1b, Supplementary Figure 1b). We next evaluated the homeostatic levels of single-strand DNA (ssDNA) in matched GICs and non-GICs as assessed by BrDU incorporation under non-denaturing conditions and detected enhanced ssDNA in GIC populations (Supplementary Figure 3b).[34,40,41] We also used the alkaline comet assay to measure DNA strand breaks. GICs had significantly longer tails and higher comet tail DNA content as compared with the non-GICs, indicating the extent of fragmented DNA at baseline was greater in the GICs (Supplementary Figure 3c–e). These observations led us to speculate that the increase in ROS levels and consequential oxidative stress to DNA might confer a GIC dependence on the SSBR pathway, the major cellular mediator of ROS, and possibly drive expression and/or activation of the SSBR initiating enzyme, PARP1. We evaluated the protein level of PARP1 and overall PARP activity, the latter assessed by poly-ADP-ribosylation (PARsylation), in matched GICs and non-GICs. GICs demonstrated markedly elevated PARsylation, the majority of which is commonly regarded to reflect PARP1 activity, across all xenografted specimens tested (Figure 1c, Supplementary Figure 4a). PARP protein levels showed a moderate or no increase in GICs (Figure 1c, Supplementary Figure 4a). We also compared the levels of PARP and PARsylation in GICs and non-GICs with normal neural progenitor cells and normal human astrocytes with GICs demonstrating the highest level of PARsylation (Supplementary Figure 4b). The purity of our GIC and non-GIC populations was confirmed by immunobloting for glial fibrillary acidic protein (GFAP), an astrocyte marker and measure of more differentiated cells, and the stem cell markers Sox2 and Olig2 (Supplementary Figure 4c). Taken together, these data demonstrate constitutive DNA damage within the GIC sub-population, triggering enhanced activation of the key SSBR player, PARP1.

PARPi preferentially targets GICs. PARPi has emerged as a promising targeted cancer therapy, yet efficacy against TICs, in general, and GICs, in particular, has not been explored. Evaluation of efficacy against the full hierarchy for those cancers defined by the cancer stem cell hypothesis is essential, as cancer stem cells may better model tumor biology than traditional cell lines. Our data suggest that GICs depend on PARP1 function, which could be therapeutically exploited. To explore this hypothesis, matched GICs and non-GICs from three independent xenografted primary patient specimens were treated with the PARP inhibitor, olaparib, and cell viability was measured over a 5-day time course. There were fewer viable cells in the GIC population following PARPi compared with non-GICs in all specimens tested (Figure 2). The efficacy of PARPi, especially in combination therapy, is more pronounced in rapidly dividing cells. To exclude the impact of differential proliferation rates on the sensitivity of the two populations to PARPi, we performed pulse labeling with the thymidine analog EdU as a measure of DNA synthesis and active proliferation. Results

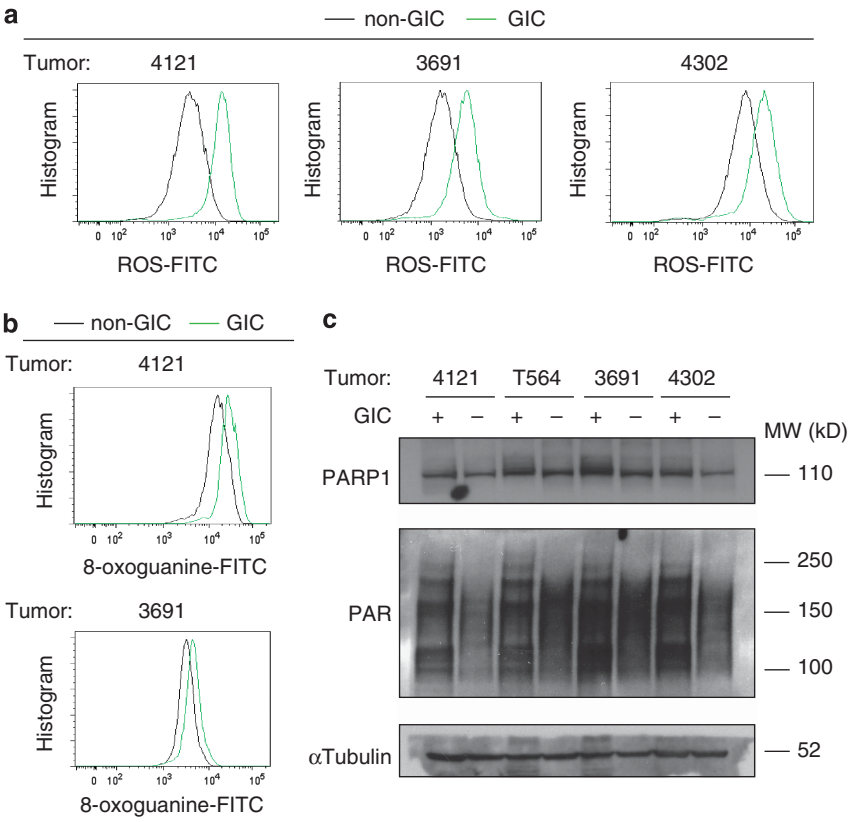

Figure 1 GICs show increased ROS levels and SSBR compared with non-GICs. (**a**) Reactive oxygen species (ROS) were measured in matched GICs (green lines) and non-GICs (black lines) from 4121, 3691, and 4302 xenografted patient specimens by flow cytometry analysis using the general oxidative stress indicator, CM-H2DCFDA. (**b**) Baseline levels of 8-oxoguanine residue (marker of oxidative damage to DNA) were assessed using OxyDNA Assay Kit in two matched GICs (green lines) and non-GICs (black lines) from acutely dissociated xenografted patient specimens (4121 and 3691). (**c**) PARP levels and PARP-associated activity (PARsylation PAR) were evaluated by immunoblot analysis of matched GICs (+) and non-GICs (−) from 4121, T564, 3691, and 4302 xenografted patient specimens

demonstrated that GICs and non-GICs were cycling with similar kinetics (Supplementary Figure 5a). In addition, both populations had similar cell cycle distribution as validated by flow cytometry for DNA content using propidium idodide (Supplementary Figure 5b). GICs and non-GICs were more sensitive to PARPi than cycling, non-neoplastic BJ fibroblasts with GICs demonstrating a significant impact on viability at all time points tested (Supplementary Figure 5c). To further confirm sensitivity of GICs to PARPi, we evaluated the sphere formation capability, a surrogate marker for self-renewal and survival, of GICs in the presence of olaparib. PARPi resulted in a significant decrease in tumorsphere formation in all specimens tested (Figure 3a, Supplementary Figure 6a and b). Colony formation was also utilized to evaluate clonogenic survival for both the GIC and non-GIC populations. Only GICs demonstrated a significant decrease in colony formation (Figure 3b and c). Similar to all small molecule inhibitors, these pharmacologic agents can have off-target effects. However, PARP1 activity as monitored by total cellular PARsylation levels correlated with olaparib treatment in GICs and non-GICs at concentrations ranging around the half maximal effective concentration (EC_{50}) for both cell types (GIC $EC_{50} = 1.20\,\mu M$; non-GIC $EC_{50} = 4.95\,\mu M$; Supplementary Figure 7a and b). These data reveal preferential sensitivity of GICs to PARPi and a dependence on PARP1 function.

PARP1 contributes to survival of GICs following irradiation. Radioresistance is a major contributor to the lethality of GBM. We therefore focused our studies on evaluating the effect of radiotherapy in combination with PARPi on the radioresistant GIC population.[2] GICs were pretreated with increasing concentrations of olaparib, with or without a single exposure to IR, and cell viability was monitored over a 10-day time course. Cells treated with radiation alone showed significant expansion by 7 days after treatment for all specimens, reinforcing a functional resistance of GICs to radiotherapy (Figure 4, right panels). Viability of GICs was completely blocked with combined PARPi and radiation (Figure 4, right panels). Olaparib monotherapy had a modest impact on GIC viability in the 10-day time course with significance consistently seen at the higher concentration for all specimens (Figure 4, left panels). We validated the efficacy of olaparib monotherapy toward GICs in combination with IR by trypan blue staining (Supplementary Figure 8). Non-GICs were also evaluated for a combinatorial effect of PARPi and radiotherapy on cell growth. Consistent with previous reports, radiotherapy alone significantly had an impact on the growth kinetics of the non-GICs more than GICs. PARPi only had an additional impact on cell viability for one specimen and only at the highest concentration evaluated *versus* the consistent impact on viability seen for the GICs (Supplementary Figure 9a). These

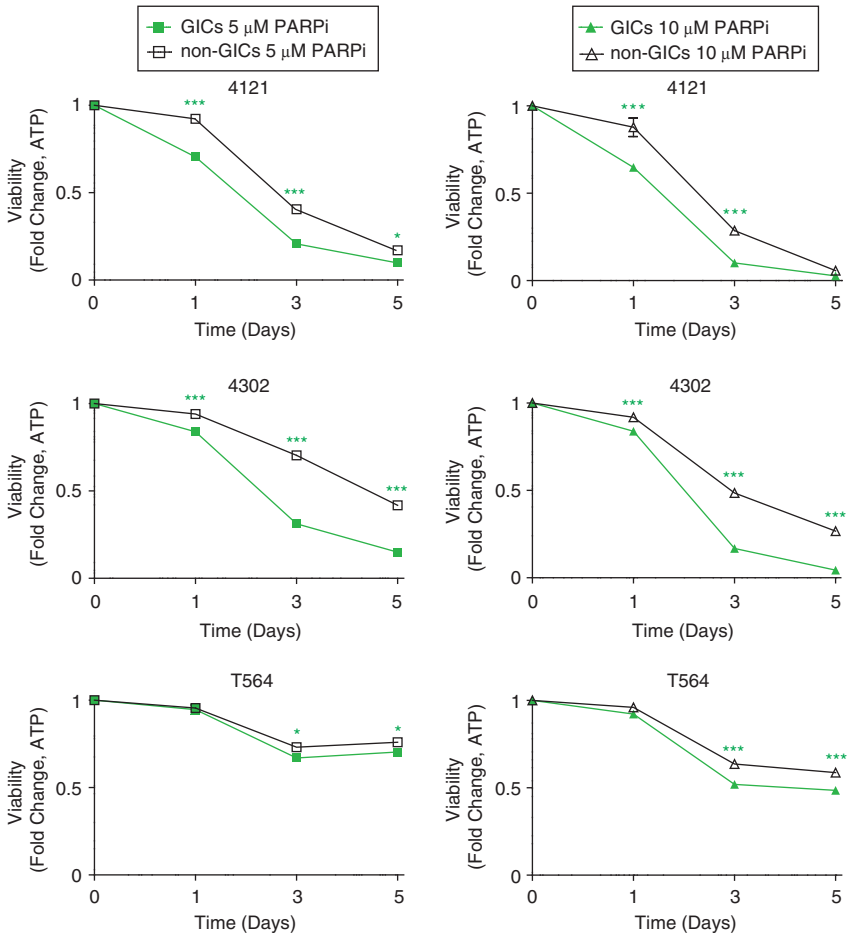

Figure 2 GICs exhibit preferential sensitivity to PARPi by olaparib. Cell viability was measured using an ATP-based assay on the indicated days for GICs (green lines) and non-GICs (black lines) from 4121, 4302, and T564 xenografted patient specimens in the presence of 5 μM (left panels) or 10 μM (right panels) olaparib (PARPi). The data for each time point were normalized to the vehicle controls. $n=3$, error bars represent S.D.; NS, no significance; $^{*}P<0.05$; $^{***}P<0.001$

results highlight an essential role for PARP1 in the GIC response to IR whereby inhibition attenuates the radio-resistant phenotype.

PARPi leads to increased apoptosis and delayed repair of DNA damage. Decreased viability of GICs following olaparib treatment prompted us to further elucidate the mechanism of cell death. GICs were treated with increasing concentrations of olaparib with or without IR, and apoptosis was measured through Caspase-3/7 activity at day 3 after treatment. In all cultures, olaparib potently increased radiation-induced apoptosis (Figure 5a). In concordance with the lack of an impact on viability, an increase in apoptosis was not seen in the non-GICs (Supplementary Figure 9b). We next evaluated repair of DNA damage induced by IR in GICs. GICs pretreated with olaparib were irradiated or left untreated and the level of DNA damage was monitored by the DNA damage marker, γH2AX. GICs resolved damaged DNA by 24 h after IR as evaluated by the loss in γH2AX signal, whereas PARPi compromised repair kinetics and/or contributed to continual formation of DNA breaks, as unrepaired ROS-induced damage can be converted to double-strand breaks (Figure 5b). Non-GICs resolved DNA damage following irradiation with the same kinetics with and without PARPi with most lesions repaired by 24 h after IR (Supplementary Figure 9c). These data suggest that PARP1 is required for GICs to respond to DNA damage and demonstrate that PARPi results in the initiation of programmed cell death in these cells.

Targeting PARP compromises the stem cell phenotype of GICs *in vitro* and *in vivo*. GICs are functionally defined by the ability to form tumorspheres from a single cell *in vitro*. The impact of a treatment on tumorsphere-forming potential of GICs can be evaluated through a limiting dilution assay, which permits quantified estimation of stem-like cell frequency. To examine the impact of olaparib in combination with IR on sphere formation, we plated GICs at single-cell densities in the presence of increasing concentrations of olaparib and evaluated tumorsphere formation 10 days later. Concomitant with its antiproliferative effects, olaparib decreased self-renewal 5–20-fold at the higher concentration (Figure 6). Self-renewal was completely inhibited with the addition of IR (Figure 6). Although cell death likely contributed to this result, the lower concentration of olaparib plus IR also demonstrated a decrease in the estimated stem

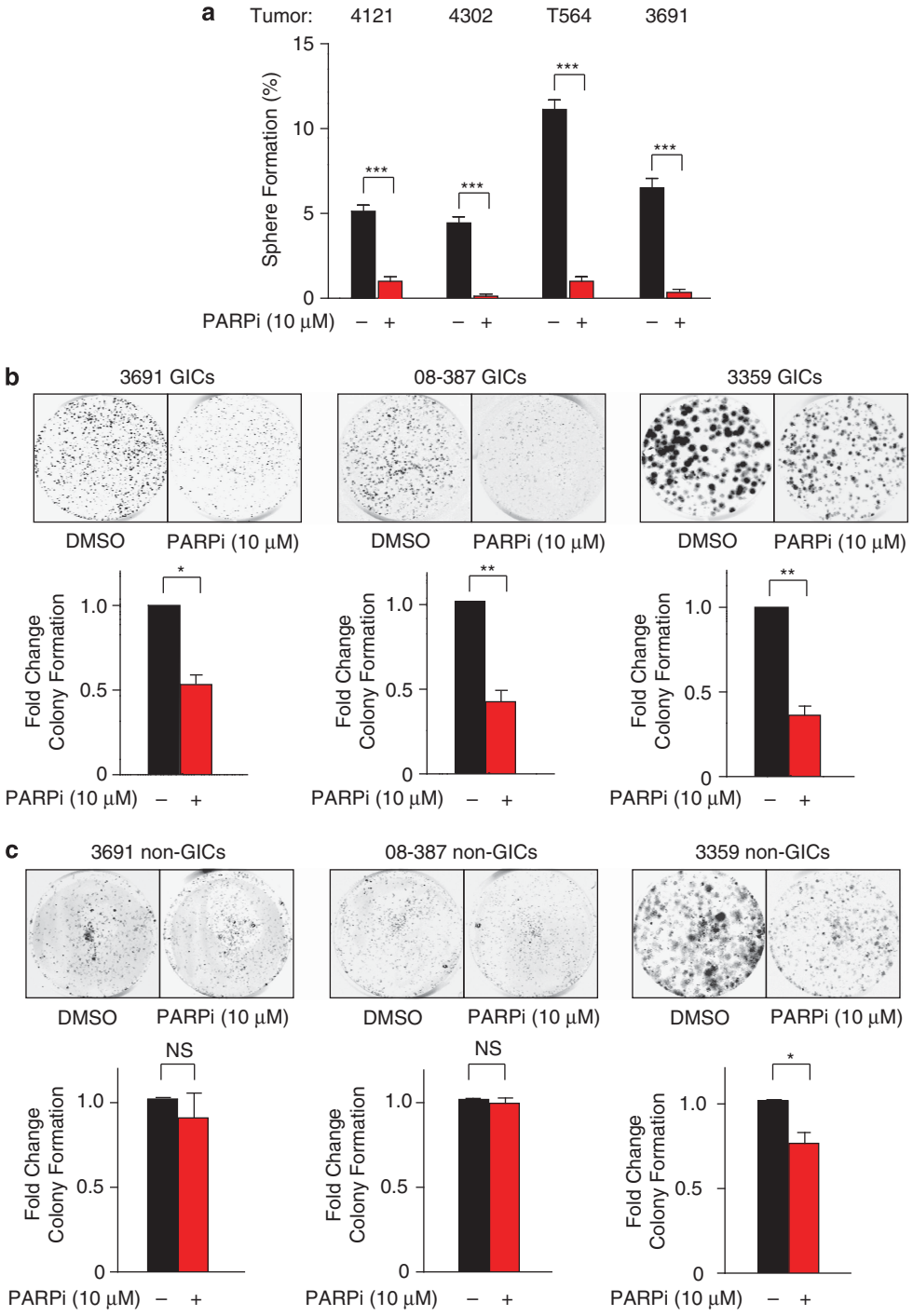

Figure 3 GICs have decreased sphere formation and viability following PARPi. (**a**) Sphere formation was evaluated for GICs from 4121, 4302, T564, and 3691 xenografted patient specimens plated in the presence (red bars) or absence (black bars) of 10 μM olaparib (PARPi). $n=3$, error bars represent S.D.; ***$P<0.001$. Clonogenic survival for GICs (**b**) and non-GICs (**c**) from 3691, 08–387, and 3359 xenografted patient specimens was evaluated by colony formation following treatment with vehicle (DMSO) or 10 μM olaparib (PARPi). Representative images of colony formation are shown in the upper panels. Fold change in colony formation in the presence (red bars) or absence (black bars) of the PARPi is shown in the bottom panels. $n=3$, error bars represent S.D.; *$P<0.05$; **$P<0.01$

cell frequency (Figure 6b). To determine any potential enhancement of the stem-reduction effect of IR due to olaparib, we calculated the expected stem cell frequencies that would occur in the combination condition if the two treatments followed a Bliss Independence model (Figure 6c). The observed values of the combination treatment were between 2.5- and 5-fold lower than would be expected because of independent effects of treatment with IR and olaparib alone, suggesting some enhancement of the radiation-induced loss of stem cell phenotype by PARPi.

As tumor initiation is the single most important TIC functional assay and GICs show greater radioresistance

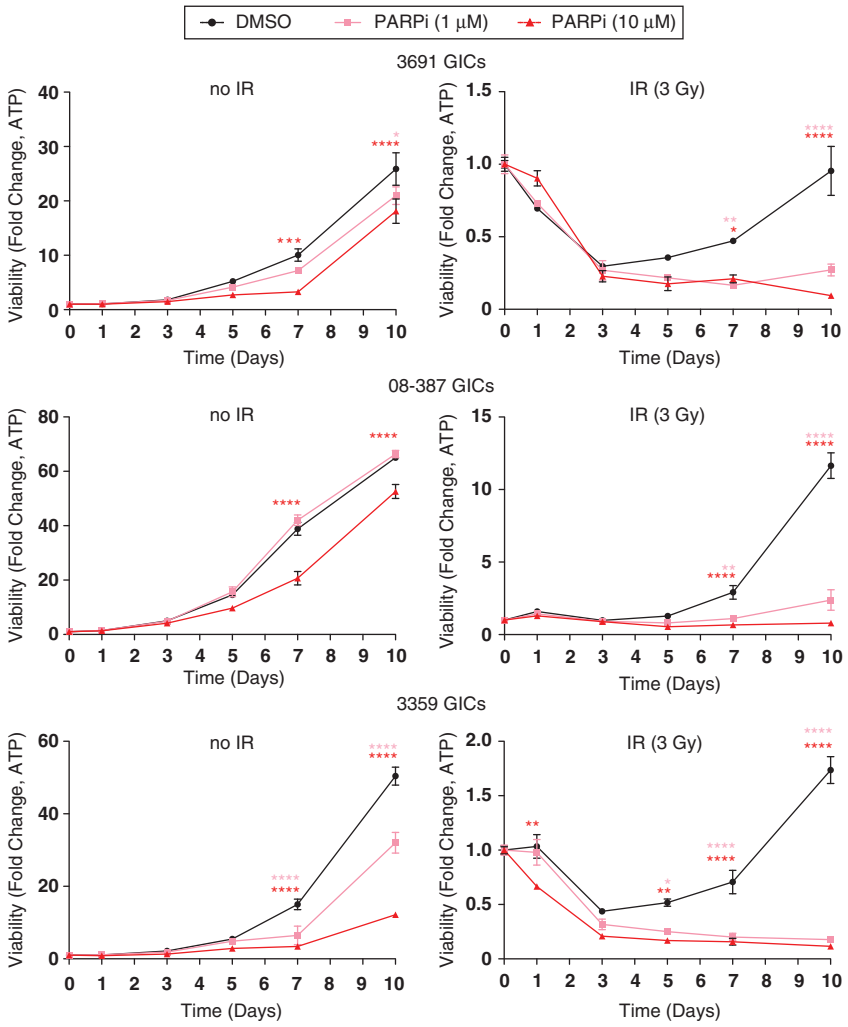

Figure 4 GICs fail to recover from irradiation following PARPi. Cell viability was measured using an ATP-based assay on the indicated days for GICs from 3691, 08–387, and 3359 xenografted patient specimens treated with vehicle (DMSO, black lines), 1 μM olaparib (PARPi, pink lines), or 10 μM olaparib (PARPi, red lines), and were left unirradiated (no IR, left panels) or irradiated with 3 Gy (right panels) of IR. The data for each time point were normalized to the day-0 readings within each treatment group and reported as a relative fold change in total moles ATP over time. $n=3$, error bars represent S.D.; *$P<0.05$; **$P<0.01$; ***$P<0.001$; ****$P<0.0001$

in vivo,[42] we interrogated olaparib efficacy *in vivo* using multiple approaches. First, we used a flank tumor growth model to test drug efficacy in the absence of delivery restrictions and to facilitate tumor isolation for quantification of GIC frequency after treatment. We utilized a 7-day inhibitor study with or without IR (Figure 7a). When tumors reached 0.12 cm^3, mice were randomized into one of four groups: vehicle only, vehicle plus IR every other day, daily PARPi, or daily PARPi before IR every other day. After 7 days, tumor weight and volume were calculated. Tumors were then immediately dissociated and evaluated the next day by flow cytometry for the percentage of CD133-positive cells, a putative GIC marker. Over the 7-day study, the only significant impact on tumor volume was seen in the olaparib plus radiotherapy group (Figure 7b). This correlated with this treatment group having the greatest fold change in tumor volume (tumor $volume_{initial}$/tumor $volume_{final}$) and weight (Figure 7c and d). As IR is reported to trigger GIC enrichment,[2,11,42] we confirmed these studies by demonstrating that in irradiated, vehicle-treated mice, the percentage of GICs nearly doubled. In contrast, the addition of olaparib significantly inhibited GIC enrichment (Figure 7e).

We next evaluated the impact of *in vivo* PARPi on stem cell function as monitored by post-treatment sphere formation. To address this, GICs isolated from the tumors from each treatment group were plated in a limiting dilution assay. Surviving GICs isolated from tumors treated with olaparib and IR had impaired stem cell function as evaluated by a reduced stem cell frequency (Figure 7f and g). Importantly, although IR alone had a significant impact on stem cell frequency within this time course, calculation of the Bliss Independence-expected stem cell frequency revealed that the inhibition of the stem cell phenotype seen by treatment with IR and PARPi is more than threefold greater than would be expected if the effects were independent (Figure 7h).

Tumor initiation is a required functional characteristic of GICs. To determine whether combinatorial treatment has an impact on tumor initiation and survival, we pretreated GICs

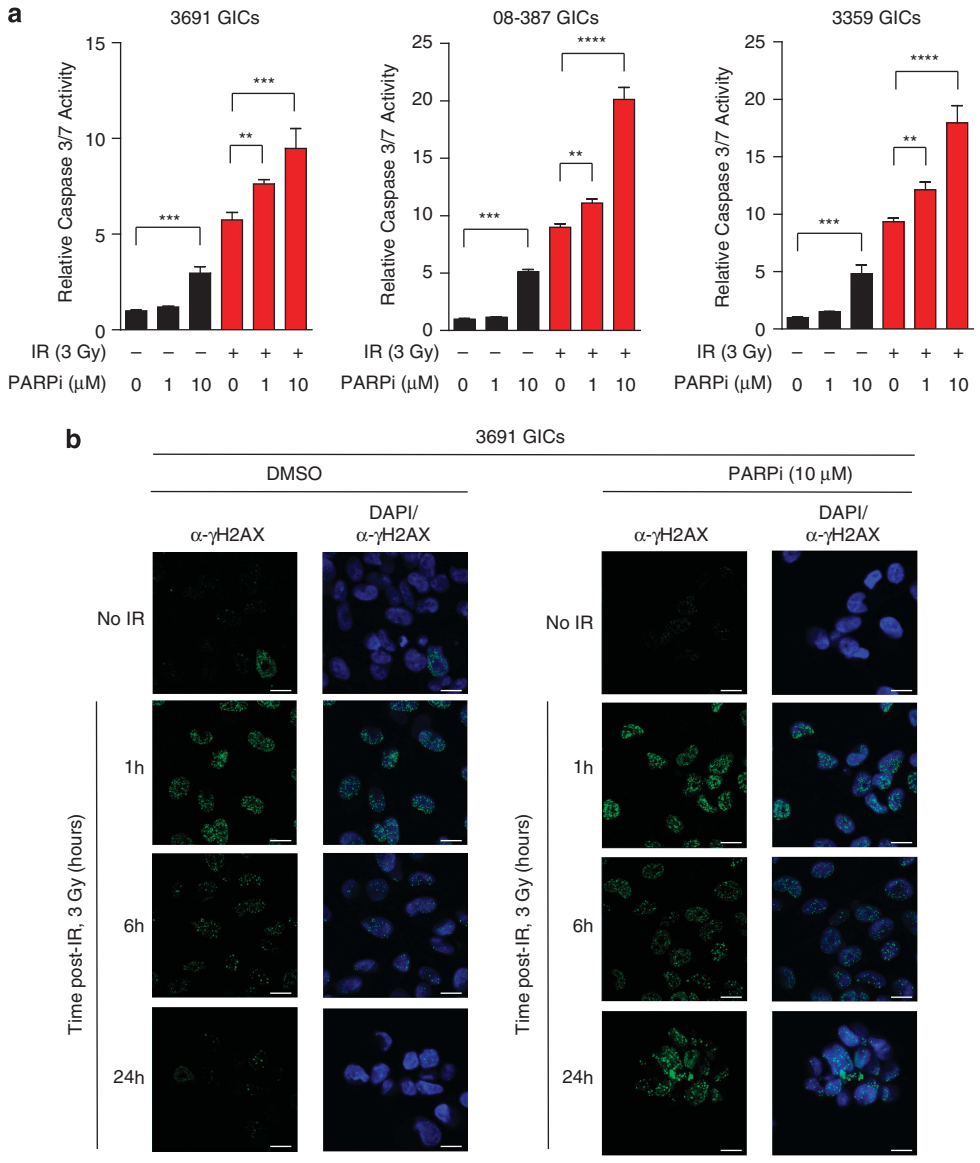

Figure 5 PARPi increases apoptosis and delays resolution of DNA damage in GICs. (**a**) Apoptosis was measured 3 days after treatment using an activated caspase-3/7-based assay for GICs from 3691, 08–387, and 3359 xenografted patient specimens treated with vehicle (DMSO), 1 μM olaparib (PARPi) or 10 μM olaparib, and were left unirradiated (black bars) or irradiated with 3 Gy of IR (red bars). The data were normalized to the unirradiated DMSO-treated controls. $n = 3$, error bars represent S.D.; $^{**}P < 0.01$; $^{***}P < 0.001$; $^{****}P < 0.0001$. (**b**) Resolution of DNA damage was monitored using immunostaining analysis for γH2AX (green; nuclei counterstained with DAPI, blue) in 3691 GICs grown as a monolayer and treated with vehicle (DMSO) or 10 μM olaparib (PARPi), and were left unirradiated (no IR) or treated with 3 Gy irradiation (IR) and fixed at the indicated time points. Scale bar = 5 μm

with vehicle or olaparib, with or without IR, and intracranially implanted viable cells into immunocompromised mice (Figure 8a). Cells treated with the inhibitor and IR showed a significant impairment of secondary tumor initiation in immunodeficient mice, further confirming a compromised stem cell phenotype (Figure 8b). Altogether, these data support the efficacy of PARPi against GICs *in vivo*, offering preclinical insight into targeting the stem cell-like population and possibly reducing tumor recurrence.

Discussion

Cure requires total cell kill. Despite the low frequency of GICs in most cancers, GICs display greater resistance to standard, cytotoxic therapies suggesting a central role in therapeutic resistance. We previously demonstrated higher basal activation of the DDR in GBM and specifically the GIC population.[2,34] We have now expanded these findings to highlight a requirement for the SSBR protein, PARP1, in GICs. Higher ROS and DNA damage within GICs likely contributes to constitutive activation of PARP1 within this population. Importantly, therapeutic exploitation of this dependence through small molecule inhibition of PARP collapses the hierarchy by reducing stem cell survival, expansion, and tumor initiation.

Our finding that GICs exhibited a higher basal level of ROS is initially surprising, given previous reports of reduced ROS in breast cancer TICs and stem-like cells from glioma cell

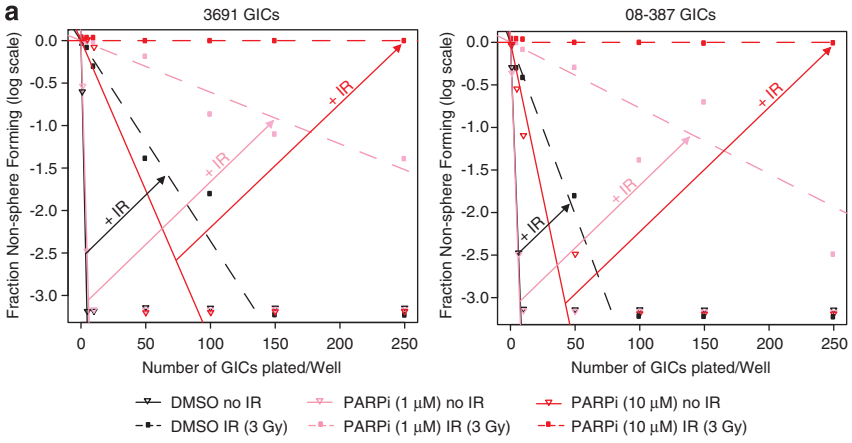

b

	Stem Cell Frequency			
	3691		08-387	
PARPi	no IR	IR (3 Gy)	no IR	IR (3 Gy)
0 μM	1 in 1.4	1 in 42.4	1 in 2.5	1 in 24.7
1 μM	1 in 1.9	1 in 164.5	1 in 2.3	1 in 129.5
10 μM	1 in 28.4	1 in ∞	1 in 13.8	1 in ∞

c

Stem Cell Frequency	3691		08-387	
	1 μM + 3 Gy	10 μM + 3 Gy	1 μM + 3 Gy	10 μM + 3 Gy
Predicted	1 in 55.1	1 in 1065.7	1 in 23.0	1 in 136.8
Actual	1 in 164.5	1 in ∞	1 in 129.5	1 in ∞
Fold Change	3.0	—	5.63	—

Figure 6 PARPi combined with radiation compromises self-renewal of GICs *in vitro*. (**a**) *In vitro* limiting dilution assay for GICs sorted from 3691 (left panel) or 08–387 (right panel) xenografted patient specimens. GICs (1, 5, 10, 50, 100, 150, or 250) were plated per well of a 96-well plate containing vehicle (DMSO, black lines), 1 μM olaparib (PARPi, pink lines) or 10 μM olaparib (PARPi, red lines), and were left unirradiated (no IR, solid lines) or irradiated with 3 Gy (dashed lines) of IR. Ten days later, each well was evaluated for the presence or absence of tumorspheres. Arrows highlight the shift in log fraction nonresponding after irradiation (+ IR). (**b**) Calculation of the estimated stem cell frequency for each condition. (**c**) Bliss Independence-predicted stem cell frequency

lines.[39,43] These differences in reported ROS levels highlight potential organ-specific metabolic states and adaptation mechanisms for TICs as well as variation generated from examining cell lines *versus* low-passage patient-derived cells.[38,44] We saw higher ATP levels in the GICs as compared with non-GICs grown in conditions that maintain similar proliferation rates, which suggest that GICs might have higher mitochondria-dependent oxidative phosphorylation directly contributing to free radical production.[43] In addition, a link between EGFR hyperactivation, a common event in GBM, and increased ROS that creates a reliance on PARP1 has been reported.[45] However, the direct mechanism leading to increased ROS in GICs is still an open area of investigation as is the overall metabolic requirements for GICs.

Nonetheless, our data indicated a higher level of oxidative base lesions and BrDU foci (ssDNA) in the GICs that were likely the direct result of ROS-induced damage. We showed that in correlation with an increase in DNA damage, there was an increase in PARsylation, which is a signal required for downstream repair factors in SSBR and additional DDR pathways. We were able to exploit the homeostatic requirement for PARP1 in GICs through PARPi followed by irradiation to eliminate GIC expansion *in vivo*, which likely contributed to the decrease in tumor growth. Further, tumor regression resulting from combinatorial treatment indicates widespread tumor efficacy owing to a direct effect on non-GICs and/or the reported antiangiogenic effect of PARPi.[46,47] Our data, however, do indicate that PARPi before irradiation compromises the ability of GICs to respond to DNA damage, driving the cells to undergo apoptosis.

In addition to cell death, PARPi compromised the stem cell phenotype, likely further attenuating GIC-mediated tumor maintenance. Although not directly tested, it is likely that the tumorigenicity of these cells was abrogated, given their compromised self-renewal capacity. When testing the tumor-initiating ability of GICs exposed to olaparib before orthotopic implantation, we found that the addition of radiation impeded their tumor-initiating capacity. These results suggest that PARPi with radiation would impair the ability of GICs to drive tumor recurrence.

Numerous agents proposed to radiosensitize cancers have shown promise in preclinical studies but have not produced substantial benefit in clinical trials. Our studies supporting use of PARP inhibitors in combination with radiation may offer potential advantages over prior agents that failed in clinical trial, as PARP inhibitors have shown acceptable toxicity in clinical trials.[33] Importantly, the ability for some PARP inhibitors to cross the blood–brain barrier has been

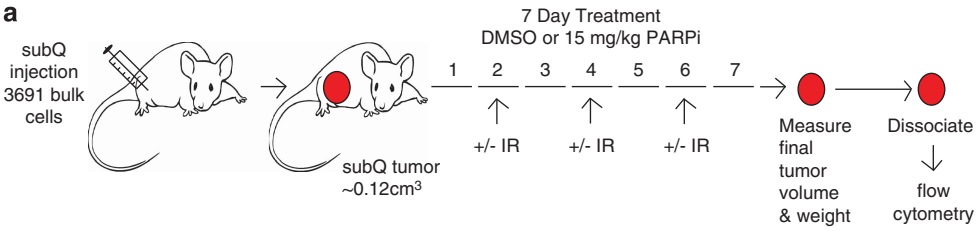

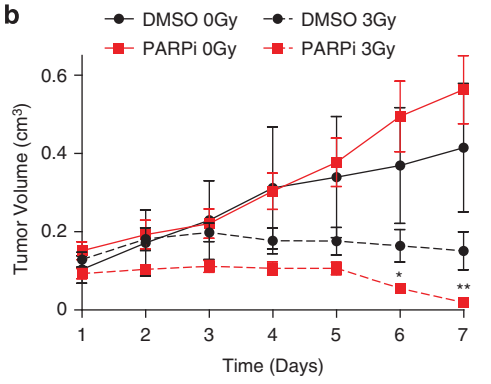

c

Average Fold Change $TV_{final}/TV_{initial}$		
In vivo treatment	no IR	IR (3 Gy)
DMSO	3.76	0.95
PARPi	3.91	0.21

d

Average Final Tumor Weight (g)		
In vivo treatment	no IR	IR (3 Gy)
DMSO	0.48	0.27
PARPi	0.52	0.06

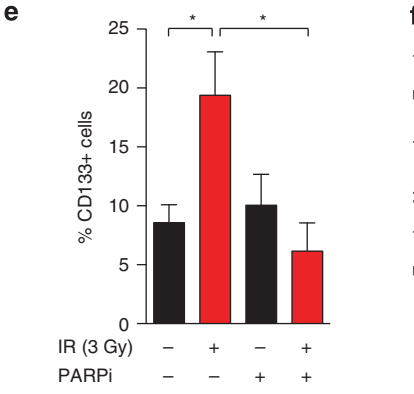

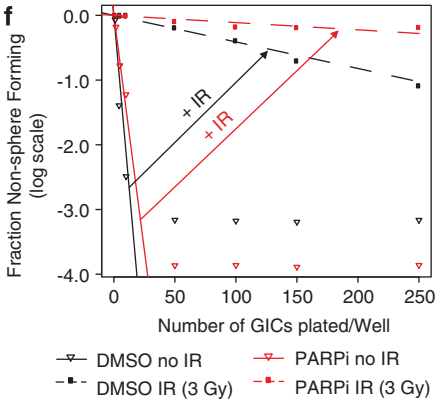

g

Stem Cell Frequency		
In vivo treatment	no IR	IR (3 Gy)
DMSO	1 in 4.7	1 in 243.7
PARPi	1 in 6.9	1 in 894.4

h

Stem Cell Frequency	In vivo treatment
	PARPi + IR (3 Gy)
Predicted	1 in 358.0
Actual	1 in 894.4
Fold Change	2.5

Figure 7 PARPi plus radiation impedes tumor growth and GIC expansion *in vivo*. (**a**) Schematic for the subcutaneous xenograft 7-day treatment paradigm. When tumors reached ~0.12 cm^3, mice were randomized into one of four treatment groups; vehicle only (DMSO; $n=4$), vehicle plus irradiation (DMSO plus 3 Gy at days 2, 4, and 6; $n=4$), 15 mg/kg olaparib only (PARPi; $n=4$), or 15 mg/kg olaparib plus irradiation (PARPi plus 3 Gy at days 2, 4, and 6; $n=5$). Tumors were measured daily and final tumor volume and weight were taken at day 7. Tumors were then dissociated and evaluated by flow cytometry for the percentage of GICs. (**b**) Line graph of the mean tumor volume over the 7-day study for each treatment group. Error bars represent S.E.M.; $^{*}P<0.05$; $^{**}P<0.01$ (**c**) Average fold change in tumor volume (tumor $volume_{final}$/tumor $volume_{inital}$) for each treatment group. (**d**) Average final tumor weight at day 7 for each treatment group. (**e**) Percentage of CD133-positive cells isolated at day 7 from each treatment group. Error bars represent S.D.; $^{*}P<0.05$. (**f**) *In vitro* limiting dilution assay for GICs sorted from subQ tumors from each treatment group. Cells (1, 5, 10, 50, 100, 150, or 250) were plated per well of a 96-well plate. Ten days later, each well was evaluated for the presence or absence of tumorspheres. Arrows highlight the shift in log fraction nonresponding after irradiation (+ IR). (**g**) Calculation of the estimated stem cell frequency for each condition. (**h**) Bliss Independence-predicted stem cell frequency

validated.[29] PARP inhibitors have been most aggressively developed in BRCA-mutant breast and ovarian cancers because of the concept of synthetic lethality: BRCA1/2-mutant cancer cells cannot compensate if both SSBR (involving PARP) and homologous recombination (involving BRCA1/2) are disrupted through a combination of pharmacologic inhibition and cellular mutation.[48] However, other solid tumors have demonstrated sensitivity to PARP inhibitors in the absence of BRCA1/2 mutations, perhaps indicating disruption in other key genotoxic stress-related pathways, including PTEN, or other unexpected mutations.[25,48–50]

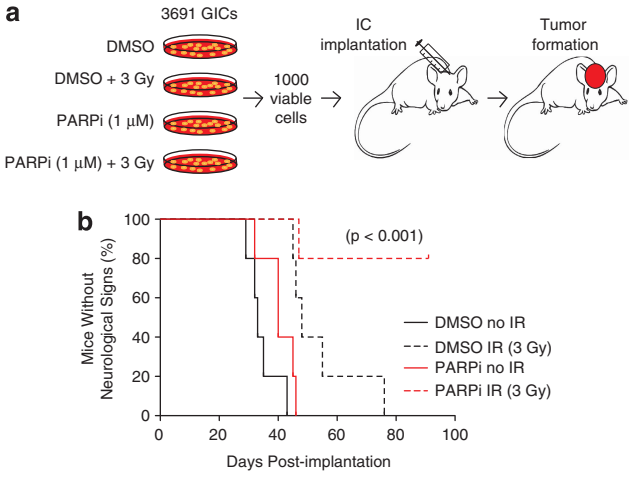

Figure 8 PARPi plus radiation compromises the stem cell phenotype *in vivo*. (**a**) Schematic for the orthotopic tumor initiation paradigm. GICs (3691) were treated with vehicle only (DMSO), vehicle plus irradiation (DMSO plus 3 Gy), 1 μM olaparib only (PARPi), or 1 μM olaparib plus irradiation (PARPi plus 3 Gy). Viable cells (1000) were intracranially implanted into the right frontal lobes of mice 2 days later ($n=5$ for each treatment). Mice were monitored daily for neurological impairment at which time they were killed and brains removed to evaluate for tumor development. (**b**) The Kaplan–Meier survival curves. Evaluation of the tumor-initiating capacity of GICs pretreated with vehicle (DMSO, solid black line; $n=5$), 1 μM olaparib (PARPi, solid red line; $n=5$), vehicle plus irradiation (DMSO plus 3 Gy, dashed black line; $n=5$), or 1 μM olaparib plus irradiation (PARPi plus 3 Gy, dashed red line; $n=5$)

Overall, the results from our studies highlight constitutive activation of PARP1 in GICs that can be therapeutically exploited and ultimately translated to clinical trials. With the appreciation of a cellular hierarchy within numerous solid tumors, and the likely contribution of the stem cell population to disease recurrence, the impact of therapies on these cells must be evaluated. A particularly promising approach might be the combination of PARPi with hypofractionated radiation to prevent cancer cells from activating compensatory survival pathways that can occur with chronic targeted therapy treatment.

Materials and Methods

Animals and *in vivo* studies. All animal studies described were approved by the Cleveland Clinic Foundation Institutional Animal Care and Use Committee and conducted in accordance with the NIH Guide for the Care and Use of Laboratory Animals. For subcutaneous tumor studies, 5×10^5 freshly dissociated GBM cells from a xenograft originally derived from a primary GBM patient specimen (3691) were injected into the flanks of 20 6–week-old male athymic Nu/Nu mice (Charles River Laboratories, Wilmington, MA, USA). Tumors were allowed to reach $\sim0.12\,cm^3$, at which point animals were randomized into four groups and treated with either vehicle control (DMSO), olaparib alone (15 mg/kg given daily by intraperitoneal injection as previously described), vehicle followed by irradiation (3 Gray (Gy)), or olaparib followed by irradiation.[50,51] Tumors were monitored and measured daily using perpendicular diameter measurements for 7 days. Tumor volume was calculated using the ellipsoid formula $\pi/6\times$ larger diameter $\times$ (smaller diameter).[2] After the last treatment on day 7, tumors were removed and weighed and then dissociated (as described below). For intracranial implantation studies, GICs were treated with vehicle or olaparib (1 μM) for 2 h and were then left unirradiated or irradiated with 3 Gy. Two days later, 1000 viable CD133-positive GICs were implanted into the right frontal lobes of athymic Nu/Nu mice. Mice were monitored daily for neurological impairment at which time they were killed and brains were removed to evaluate for tumor development.

Isolation and culture of CD133-positive GICs. Human tissues were acquired from primary human brain tumor patient specimens in accordance with appropriate approved Institutional Review Board protocols. Tumor grade and available cytogenetic information for each specimen has been previously described.[35] Tumor specimens were maintained through subcutaneous xenografts in the flanks of athymic Nu/Nu mice. Tumors were dissociated using a papain dissociation system (Worthington Biochemical, Lakewood, NJ, USA). CD133-positive cells were enriched either by FACS or magnetic-activated cell sorting as per the manufacturer's recommendations (MACS; Miltenyi Biotec, Bergisch Gladbach, Germany) and grown as tumorspheres. All cells were cultured at 37 °C in an atmosphere of 5% CO_2. GICs were cultured in Neurobasal media (Invitrogen, Carlsbad, CA, USA) with B27 (without Vitamin A; Invitrogen), basic fibroblast growth factor (10 ng/ml; R&D Systems, Minneapolis, MN, USA), epidermal growth factor (10 ng/ml; R&D Systems), L-glutamine (2 mM; Invitrogen), and sodium pyruvate (1 mM; Invitrogen). For cell counting before each experiment, a single-cell suspension was achieved using TrypLE (Invitrogen).

Immunoblotting. RIPA protein extracts from human GBM-xenografted specimens were separated by 3–8% Novex NuPAGE SDS-PAGE Gel System (Invitrogen) and transferred to nitrocellulose membranes (Advantech, Dublin, CA, USA) using the iBlot System (Invitrogen). The membranes were blocked with 5% (wt/vol) dry milk in PBS-Tween-20 (0.5% vol/vol) and probed with primary antibodies against PARP1 (1 : 200; BD Pharmingen, San Jose, CA, USA), poly (ADP-Ribose) (PAR; 1 : 2000; BD Pharmingen), GFAP (1 : 10 000; DAKO, Santa Clara, CA, USA), or α-tubulin (1 : 500; Sigma-Aldrich, St. Louis, MO, USA) as a loading control. ECL detection system was used according to the manufacturer's instructions (GE Healthcare, Little Chalfont, UK).

Irradiation. Cells and subcutaneous tumors were irradiated in a JL Shepherd Mark I ^{137}Cs irradiator (San Fernando, CA, USA). Mice were anesthetized and all but the subcutaneous tumor was shielded with lead during delivery, given on days 2, 4, and 6 of the 7-day experiment. In all studies, 3 Gy was delivered 2 h after vehicle or drug treatment.

Small molecule inhibitors. The PARP inhibitor (olaparib; Selleck Chemicals, Houston, TX, USA) was resuspended in DMSO. For *in vivo* studies, olaparib was diluted in (2-hydroxypropyl)-β-cyclodextrin (Sigma-Aldrich) in phosphate-buffered saline as previously described.[51] DMSO at a final percentage equivalent to that of the drug suspensions served as the vehicle control for all studies.

Colony formation assay. Colony formation assays for GICs were performed as previously described.[2] Briefly, GICs were plated in triplicate and treated with vehicle control (DMSO) or olaparib (10 μM) in supplemented neurobasal medium (3000 cells per well). Six days later, upon visible colony/tumorsphere formation, 5% FBS was added per well to allow for the colonies to adhere, and plates were processed 48 h later. Non-GICs were plated in triplicate and treated with vehicle control (DMSO) or olaparib (10 μM) in Dulbecco's modified Eagle medium, 10% FBS (3000 cells per well). Cell colonies were fixed with methanol and stained with a 0.5% crystal violet solution. Plates were imaged using plate-scanning software on an inverted microscope (Leica, Wetzlar, Germany). An area threshold of 500 pixels (equivalent to a colony of $\sim$50 cells) was set and a total area positive for colony formation was calculated for each plate.

Cell viability and apoptosis assays. To measure the putative differential sensitivity of GICs *versus* non-GICs to PARPi, acutely dissociated and CD133-MACS sorted GBM cells (6000 cells per well of a 96-well plate, plated in triplicate) were exposed to olaparib (5 or 10 μM) in growth factor-free medium (Neurobasal A medium supplemented with B27 minus vitamin A) and viability was measured at day 0 and days 1, 3, and 5 post treatment using CellTiter-Glo Luminescent Cell Viability Assay (Promega, Madison, WI, USA). Results are reported as relative fold change in ATP with each group internally normalized to the respective vehicle control. For long-term viability assays, 500 GICs per well were plated in triplicate into 96-well plates containing appropriate growth media. The next day, vehicle or drug was added to the wells and 2 h later plates were irradiated or left untreated. Day-0 readings of ATP levels (CellTiter-Glo Luminescent Cell Viability Assay, Promega) were taken immediately after irradiation using a luminometer (Perkin-Elmer, Waltham, MA, USA). ATP levels were also taken on days 1, 3, 5, 7, and 10, and normalized within each treatment group to day-0 readings and reported as

a relative fold change in total moles ATP over time. GICs and non-GIC were grown in growth factor-free medium as described above, and apoptosis was evaluated by measuring the activity of caspase-3 and -7 (Caspase-Glo 3/7, Promega), normalized to total cell viability within that treatment group as measured by CellTiter-Glo, on day 3 following the same treatment set-up as the ATP assay.

Immunofluorescence imaging. Detection of γH2AX (1 : 500; Abcam, Cambridge, UK) was performed as described previously.[34,40] GICs and non-GICs were grown on GelTrex (Gibco, Invitrogen, Carlsbad, CA, USA)-coated cover slips and treated with DMSO or 10 μM olaparib and left unirradiated or irradiated with 3 Gy and fixed 1, 6, or 24 h after irradiation. Cells were then immunostained for γH2AX. Secondary detection was accomplished using Alexa Fluor 488 goat anti-mouse IgG (Invitrogen). Nuclei were counterstained with DAPI. Imaging was performed using the LSM 510 META/Imager.Z1 (Plan-Apochromat 63 $\times$ /1.40 oil DIC M27 objective; Carl Zeiss, Inc., Oberkochen, Germany). Confocal images were acquired with equal settings and processed with Zen 2008 software (Carl Zeiss, Inc.).

Flow cytometric analysis and sorting. Flow cytometry was performed using a FACS Aria II Cell Sorter (BD Biosciences, Franklin Lakes, NJ, USA). To enrich for CD133-positive GICs, single cells were labeled with an allophycocyanin-conjugated monoclonal antibody against CD133 (CD133/2; Miltenyi Biotec). Only live cells were selected for through negative staining for propidium iodide. Isotype controls were used to establish proper gates.

Flow cytometry analysis of ROS and 8-oxoguanosin. Quantification of ROS and 8-oxoguanosin was measured as described previously.[34] In detail, acutely dissociated xenografts were left to recover and MACS sorted within 12 h after dissociation. Two hours after the MACS sort, matched GICs and non-GICs were dissociated using accutase and stained with CM-H2DCFDA probe according to the manufacturer's instructions (Molecular Probes, Invitrogen, Carlsbad, CA, USA), acquired with FACSVerse (BD Biosciences), and analyzed using FlowJo software (Tree Star, Inc., Ashland, OR, USA). Calbiochem (Merck KGaA, Darmstadt, Germany) OxyDNA Kit was used to evaluate the presence of 8-oxoguanine moiety of 8-oxoguanosine in oxidized DNA in matched GICs and non-GICs, prepared as described above for ROS measurement. BD Fortessa (BD Biosciences) and FlowJo software were used for data acquisition and analysis.

Limiting dilution assay and sphere formation. CD133-positive GICs from acutely dissociated patient xenograft specimens were flow sorted, as described, into 96-well plates at a final cell number per well of 1 (24 wells per plate), 5, 10, 50, 100, 150, or 250 (all at 12 wells per plate). For limiting dilution assays performed on cells isolated from *in vivo* inhibitor studies, cells were sorted into wells containing supplemented Neurobasal media (Invitrogen, Carlsbad, CA, USA), as described above. For all other limiting dilution assays, cells were sorted into supplemented Neurobasal media containing vehicle control (DMSO) or olaparib (1 or 10 μM). Tumorsphere formation was evaluated 10 days after sorting and wells were scored positive or negative for the presence of at least one tumorsphere. The estimated stem cell frequency was calculated using extreme limiting dilution analysis.[52] For percent sphere formation, 200 GICs were plated per well of a 12-well plate, and sphere formation was calculated using the formula: sphere formation (%) = (number of spheres/number of cells plated) $\times$ 100.

Statistical analysis. Statistical significance was calculated with GraphPad Prism Software utilizing a one-way or two-way ANOVA with a Bonferroni's *post hoc* test, Student's *t*-test, or log-rank (Mantel–Cox) test, where appropriate (GraphPad Software Inc., San Diego, CA, USA). Data are represented as the mean $\pm$ S.D. For calculation of predicted stem frequencies following treatment with olparib and IR, a Bliss independence model was utilized.[53,54] Bliss independence assumes no interaction between treatments; thus, the fractional response caused by treatment with a combination of olparib and IR would be equal to the product of the fractional responses of each treatment independently.

Conflict of Interest

The authors declare no conflict of interest.

Acknowledgements. We thank our funding sources: the National Institutes of Health Grants CA154130, CA169117 and CA1129958 (JNR) and CA151522 (ABH), American Brain Tumor Association (MV and LS), and James S McDonnell Foundation (JNR). The Danish Council for Independent Research/Medical Sciences ID4765/11-105457 (PH); Czech Ministry of Health (NT11065-5); European Commission (projects Infla-Care, CZ.1.07/2.3.00/20.0019, CZ.1.05/2.1.00/01.0030, DDResponse); the Danish National Research Foundation, the Novo Nordisk Foundation, and the Lundbeckfonden. We appreciate critical manuscript review by D Schonberg, K Sukhdeo, M Rivera, M Summers, J Lathia, and J Liu; flow cytometry assistance by C Shemo, S O'Bryant, and M Morgan; imaging assistance by J Drazba, E Diskin, and Pavel Moudry; and animal support provided by the Lerner Research Institute BRU.

1. Stupp R, Hegi ME, Neyns B, Goldbrunner R, Schlegel U, Clement PM *et al.* Phase I/IIa study of cilengitide and temozolomide with concomitant radiotherapy followed by cilengitide and temozolomide maintenance therapy in patients with newly diagnosed glioblastoma. *J Clin Oncol* 2010; **28**: 2712–2718.
2. Bao S, Wu Q, McLendon RE, Hao Y, Shi Q, Hjelmeland AB *et al.* Glioma stem cells promote radioresistance by preferential activation of the DNA damage response. *Nature* 2006; **444**: 756–760.
3. Galli R, Binda E, Orfanelli U, Cipelletti B, Gritti A, De Vitis S *et al.* Isolation and characterization of tumorigenic, stem-like neural precursors from human glioblastoma. *Cancer Res* 2004; **64**: 7011–7021.
4. Hemmati HD, Nakano I, Lazareff JA, Masterman-Smith M, Geschwind DH, Bronner-Fraser M *et al.* Cancerous stem cells can arise from pediatric brain tumors. *Proc Natl Acad Sci USA* 2003; **100**: 15178–15183.
5. Ignatova TN, Kukekov VG, Laywell ED, Suslov ON, Vrionis FD, Steindler DA. Human cortical glial tumors contain neural stem-like cells expressing astroglial and neuronal markers in vitro. *Glia* 2002; **39**: 193–206.
6. Singh SK, Clarke ID, Terasaki M, Bonn VE, Hawkins C, Squire J *et al.* Identification of a cancer stem cell in human brain tumors. *Cancer Res* 2003; **63**: 5821–5828.
7. Singh SK, Hawkins C, Clarke ID, Squire JA, Bayani J, Hide T *et al.* Identification of human brain tumour initiating cells. *Nature* 2004; **432**: 396–401.
8. Liu G, Yuan X, Zeng Z, Tunici P, Ng H, Abdulkadir IR *et al.* Analysis of gene expression and chemoresistance of CD133 + cancer stem cells in glioblastoma. *Mol Cancer* 2006; **5**: 67.
9. Bao S, Wu Q, Sathornsumetee S, Hao Y, Li Z, Hjelmeland AB *et al.* Stem cell-like glioma cells promote tumor angiogenesis through vascular endothelial growth factor. *Cancer Res* 2006; **66**: 7843–7848.
10. Cheng L, Wu Q, Guryanova OA, Huang Z, Huang Q, Rich JN *et al.* Elevated invasive potential of glioblastoma stem cells. *Biochem Biophys Res Commun* 2011; **406**: 643–648.
11. Tamura K, Aoyagi M, Wakimoto H, Ando N, Nariai T, Yamamoto M *et al.* Accumulation of CD133-positive glioma cells after high-dose irradiation by Gamma Knife surgery plus external beam radiation. *J Neurosurg* 2010; **113**: 310–318.
12. Zhou BB, Zhang H, Damelin M, Geles KG, Grindley JC, Dirks PB. Tumour-initiating cells: challenges and opportunities for anticancer drug discovery. *Nat Rev Drug Discov* 2009; **8**: 806–823.
13. Pajonk F, Vlashi E, McBride WH. Radiation resistance of cancer stem cells: the 4 R's of radiobiology revisited. *Stem Cells* 2010; **28**: 639–648.
14. Chang CJ, Hsu CC, Yung MC, Chen KY, Tzao C, Wu WF *et al.* Enhanced radiosensitivity and radiation-induced apoptosis in glioma CD133-positive cells by knockdown of SirT1 expression. *Biochem Biophys Res Commun* 2009; **380**: 236–242.
15. Wang J, Wakeman TP, Lathia JD, Hjelmeland AB, Wang XF, White RR *et al.* Notch promotes radioresistance of glioma stem cells. *Stem Cells* 2010; **28**: 17–28.
16. Yang YP, Chang YL, Huang PI, Chiou GY, Tseng LM, Chiou SH *et al.* Resveratrol suppresses tumorigenicity and enhances radiosensitivity in primary glioblastoma tumor initiating cells by inhibiting the STAT3 axis. *J Cell Physiol* 2012; **227**: 976–993.
17. Hamerlik P, Lathia JD, Rasmussen R, Wu Q, Bartkova J, Lee M *et al.* Autocrine VEGF-VEGFR2-Neuropilin-1 signaling promotes glioma stem-like cell viability and tumor growth. *J Exp Med* 2012; **209**: 507–520.
18. Facchino S, Abdouh M, Chatoo W, Bernier G. BMI1 confers radioresistance to normal and cancerous neural stem cells through recruitment of the DNA damage response machinery. *J Neurosci* 2010; **30**: 10096–10111.
19. Cheng L, Wu Q, Huang Z, Guryanova OA, Huang Q, Shou W *et al.* L1CAM regulates DNA damage checkpoint response of glioblastoma stem cells through NBS1. *EMBO J* 2011; **30**: 800–813.
20. Svendsen A, Verhoeff JJ, Immervoll H, Brogger JC, Kmiecik J, Poli A *et al.* Expression of the progenitor marker NG2/CSPG4 predicts poor survival and resistance to ionising radiation in glioblastoma. *Acta Neuropathol* 2011; **122**: 495–510.
21. Calabrese CR, Almassy R, Barton S, Batey MA, Calvert AH, Canan-Koch S *et al.* Anticancer chemosensitization and radiosensitization by the novel poly(ADP-ribose) polymerase-1 inhibitor AG14361. *J Natl Cancer Inst* 2004; **96**: 56–67.
22. Chalmers A, Johnston P, Woodcock M, Joiner M, Marples B. PARP-1, PARP-2, and the cellular response to low doses of ionizing radiation. *Int J Radiat Oncol Biol Phys* 2004; **58**: 410–419.
23. Dungey FA, Caldecott KW, Chalmers AJ. Enhanced radiosensitization of human glioma cells by combining inhibition of poly(ADP-ribose) polymerase with inhibition of heat shock protein 90. *Mol Cancer Ther* 2009; **8**: 2243–2254.

24. Dungey FA, Loser DA, Chalmers AJ. Replication-dependent radiosensitization of human glioma cells by inhibition of poly(ADP-Ribose) polymerase: mechanisms and therapeutic potential. *Int J Radiat Oncol Biol Phys* 2008; **72**: 1188–1197.
25. Oplustilova L, Wolanin K, Mistrik M, Korinkova G, Simkova D, Bouchal J *et al.* Evaluation of candidate biomarkers to predict cancer cell sensitivity or resistance to PARP-1 inhibitor treatment. *Cell Cycle* 2012; **11**: 20.
26. Russo AL, Kwon HC, Burgan WE, Carter D, Beam K, Weizheng X *et al.* In vitro and in vivo radiosensitization of glioblastoma cells by the poly (ADP-ribose) polymerase inhibitor E7016. *Clin Cancer Res* 2009; **15**: 607–612.
27. van Vuurden DG, Hulleman E, Meijer OL, Wedekind LE, Kool M, Witt H *et al.* PARP inhibition sensitizes childhood high grade glioma, medulloblastoma and ependymoma to radiation. *Oncotarget* 2011; **2**: 984–996.
28. Albert JM, Cao C, Kim KW, Willey CD, Geng L, Xiao D *et al.* Inhibition of poly(ADP-ribose) polymerase enhances cell death and improves tumor growth delay in irradiated lung cancer models. *Clin Cancer Res* 2007; **13**: 3033–3042.
29. Donawho CK, Luo Y, Penning TD, Bauch JL, Bouska JJ, Bontcheva-Diaz VD *et al.* ABT-888, an orally active poly(ADP-ribose) polymerase inhibitor that potentiates DNA-damaging agents in preclinical tumor models. *Clin Cancer Res* 2007; **13**: 2728–2737.
30. Kelland LR, Tonkin KS. The effect of 3-aminobenzamide in the radiation response of three human cervix carcinoma xenografts. *Radiother Oncol* 1989; **15**: 363–369.
31. Khan K, Araki K, Wang D, Li G, Li X, Zhang J *et al.* Head and neck cancer radiosensitization by the novel poly(ADP-ribose) polymerase inhibitor GPI-15427. *Head Neck* 2010; **32**: 381–391.
32. Senra JM, Telfer BA, Cherry KE, McCrudden CM, Hirst DG, O'Connor MJ *et al.* Inhibition of PARP-1 by olaparib (AZD2281) increases the radiosensitivity of a lung tumor xenograft. *Mol Cancer Ther* 2011; **10**: 1949–1958.
33. Underhill C, Toulmonde M, Bonnefoi H. A review of PARP inhibitors: from bench to bedside. *Ann Oncol* 2011; **22**: 268–279.
34. Bartkova J, Hamerlik P, Stockhausen MT, Ehrmann J, Hlobilkova A, Laursen H *et al.* Replication stress and oxidative damage contribute to aberrant constitutive activation of DNA damage signalling in human gliomas. *Oncogene* 2010; **29**: 5095–5102.
35. Eyler CE, Wu Q, Yan K, MacSwords JM, Chandler-Militello D, Misuraca KL *et al.* Glioma stem cell proliferation and tumor growth are promoted by nitric oxide synthase-2. *Cell* 2011; **146**: 53–66.
36. Lathia JD, Gallagher J, Heddleston JM, Wang J, Eyler CE, Macswords J *et al.* Integrin alpha 6 regulates glioblastoma stem cells. *Cell Stem Cell* 2010; **6**: 421–432.
37. Li Z, Bao S, Wu Q, Wang H, Eyler C, Sathornsumetee S *et al.* Hypoxia-inducible factors regulate tumorigenic capacity of glioma stem cells. *Cancer Cell* 2009; **15**: 501–513.
38. Lee J, Kotliarova S, Kotliarov Y, Li A, Su Q, Donin NM *et al.* Tumor stem cells derived from glioblastomas cultured in bFGF and EGF more closely mirror the phenotype and genotype of primary tumors than do serum-cultured cell lines. *Cancer Cell* 2006; **9**: 391–403.
39. Diehn M, Cho RW, Lobo NA, Kalisky T, Dorie MJ, Kulp AN *et al.* Association of reactive oxygen species levels and radioresistance in cancer stem cells. *Nature* 2009; **458**: 780–783.
40. Groth A, Corpet A, Cook AJ, Roche D, Bartek J, Lukas J *et al.* Regulation of replication fork progression through histone supply and demand. *Science* 2007; **318**: 1928–1931.
41. Raderschall E, Golub EI, Haaf T. Nuclear foci of mammalian recombination proteins are located at single-stranded DNA regions formed after DNA damage. *Proc Natl Acad Sci USA* 1999; **96**: 1921–1926.
42. Jamal M, Rath BH, Tsang PS, Camphausen K, Tofilon PJ. The brain microenvironment preferentially enhances the radioresistance of CD133(+) glioblastoma stem-like cells. *Neoplasia* 2012; **14**: 150–158.
43. Vlashi E, Lagadec C, Vergnes L, Matsutani T, Masui K, Poulou M *et al.* Metabolic state of glioma stem cells and nontumorigenic cells. *Proc Natl Acad Sci USA* 2011; **108**: 16062–16067.
44. Le Belle JE, Orozco NM, Paucar AA, Saxe JP, Mottahedeh J, Pyle AD *et al.* Proliferative neural stem cells have high endogenous ROS levels that regulate self-renewal and neurogenesis in a PI3K/Akt-dependant manner. *Cell Stem Cell* 2011; **8**: 59–71.
45. Nitta M, Kozono D, Kennedy R, Stommel J, Ng K, Zinn PO *et al.* Targeting EGFR induced oxidative stress by PARP1 inhibition in glioblastoma therapy. *PLoS One* 2010; **5**: e10767.
46. Martin-Oliva D, Aguilar-Quesada R, O'Valle F, Munoz-Gamez JA, Martinez-Romero R, Garcia Del Moral R *et al.* Inhibition of poly(ADP-ribose) polymerase modulates tumor-related gene expression, including hypoxia-inducible factor-1 activation, during skin carcinogenesis. *Cancer Res* 2006; **66**: 5744–5756.
47. Tentori L, Lacal PM, Muzi A, Dorio AS, Leonetti C, Scarsella M *et al.* Poly(ADP-ribose) polymerase (PARP) inhibition or *PARP-1* gene deletion reduces angiogenesis. *Eur J Cancer* 2007; **43**: 2124–2133.
48. Lord CJ, Ashworth A. The DNA damage response and cancer therapy. *Nature* 2012; **481**: 287–294.
49. Garnett MJ, Edelman EJ, Heidorn SJ, Greenman CD, Dastur A, Lau KW *et al.* Systematic identification of genomic markers of drug sensitivity in cancer cells. *Nature* 2012; **483**: 570–575.
50. Mendes-Pereira AM, Martin SA, Brough R, McCarthy A, Taylor JR, Kim JS *et al.* Synthetic lethal targeting of PTEN mutant cells with PARP inhibitors. *EMBO J Mol Med* 2009; **1**: 315–322.
51. Farmer H, McCabe N, Lord CJ, Tutt AN, Johnson DA, Richardson TB *et al.* Targeting the DNA repair defect in BRCA mutant cells as a therapeutic strategy. *Nature* 2005; **434**: 917–921.
52. Hu Y, Smyth GK. ELDA: extreme limiting dilution analysis for comparing depleted and enriched populations in stem cell and other assays. *J Immunol Methods* 2009; **347**: 70–78.
53. Bliss CI. The toxicity of poisons applied jointly. *Ann Appl Biol* 1939; **26**: 585–615.
54. Greco WR, Bravo G, Parsons JC. The search for synergy: a critical review from a response surface perspective. *Pharmacol Rev* 1995; **47**: 331–385.

Supplementary Information accompanies this paper on Cell Death and Differentiation website (http://www.nature.com/cdd)